Transactions of the Korean Society of Mechanical Engineers, Vol. 6, No. 2, pp. 147~159, 1982. 147

<Original>

Patterns of Natural Convection around a Square Cylinder Placed Concentrically in a Horizontal Circular Cylinder

K. S. Chang* and Y. H. Won**

(Received Octover 27, 1981)

水平圓管 內部에 位置한 同軸正方形 물체 주위에서의 自然對流持性

蔣 根 植 · 元 永 浩

抄 錄

內部에 正方形, 外部에 圓形인 두 定溫同心水平管으로 이루어진 폐쇄공간에서 熱浮力으로 야기된 對流熱傳達 현상을 연구하였다. 주어진 非定規的 형상에서의 층류定常 Boussinesq 유동을 해석하기 위하여, 地球重力方向에 대하여 가능한 두개의 대칭형 위치에 관하여, Galerkin 有限要素法을 사용하였다. 理論의 結果를 確證하기 위하여 실험적으로도 온도측정과 流線의 可視化를 수행하였다. 正方形內管의 直角인 線端은 局所 및 總體熱傳達에 있어서 소극적인 역활을 하지만, 이들로 因한 경계층 유동의 剝離는 발생하지 아니함을 보였다. 이 內管의 上部 水平面上에서는 유동속도와 온도勾配가 낮기는 하나 確然한 대칭형의 熱上昇流(Plume)가 가능하였다. 內管의 壁面들이 地球重力方向에 關하여 ±45°의 角을 이룰 경우 渦流의 中心部가, Rayleigh 數가 6.5×10^4 보다 작을 때는 4개, 이보다 클때는 2개가 폐쇄공간 안에서 발생하였다.

Nomenclature

- a : Half of the height of the inner square cylinder
- g : Gravitational acceleration vector
- k : Thermal conductivity of the fluid
- l_x : Cosine of angle between x-axis and gravity force g
- l_y : Cosine of angle between y-axis and gravity force g
- n : Coordinate in the direction normal to a boundary
- p : Scaled static pressure, see above of Eq. (1)
- q : Local heat flux, $k\partial T^*/\partial n^*$
- x, y : Dimensionless cartesian coordinate in horizontal and vertical directions respectively; see above of Eq. (1)
- x : Vector of unknown nodal variables
- u, v : Velocity component in x-and y-directions, scaled; see above of Eq. (1)
- u : Velocity vector
- A_e : Domain of element area
- C : Convective Matrix, see Eq. (13)

* Member, Korea Advanced Institute of Science and Technology.

** Research and Development Engineer, Daewoo Shipbuilding Industry, Inc.

F : Force vector, see Eq. (13)
G_r : Grashof number, $g\beta R^3(T_i-T_0)/\nu^2$
K : Diffusive matrix, see Eq. (13)
K_e : Local equivalent conductivity, see Eq. (21)
L : A characteristic distance, R-a
$M(x,y)$: Shape function of linear form
$N(x,y)$: Shape function of quadratic form
P_r : Prandtl number, ν/α
R : Radius of the outer circular cylinder
R_a : Rayleigh number, $g\beta R^3\ (T_i-T_0)/\nu\alpha$
S : Surface area of the inner or outer cylinder which is scaled
S_e : Domain of element boundary
T : Scaled temperature; see above of Eq. (1)
T_i, T_0 : Dimensional temperature along the inner and outer cylinders
α : Thermal diffusivity of a fluid
β : Volumetric thermal expansion coefficient
ϕ : Azimuthal angle of the outer circular cylinder
μ : Viscosity
ν : Kinematic viscosity
ρ_0 : Density taken constant at a mean temperature of the convection enclosure

Superscript

* refers to the dimensional form

Subscripts

i, j, k : Indices used for nodal points in an element

1. Introduction

Extensive studies have been made on natural convection heat transfer about relatively simple configurations for which convenient natural coordinate systems exist. They include buoyancy-driven flows about circular cylinders, spherical or elliptic bodies of revolution, flat plates, rectangular cavities and enclosures, triangles, concentric or eccentric circular annuli and spherical shells. In the present paper, study has been made on the laminar natural convection heat transfer from an inner isothermal horizontal square cylinder to an outer concentric circular cylinder, which is placed at a lower but constant temperature. Although the flow geometry appears unusal, this study is important in understanding how a thermal boundary layer develops past sharp edges of the inner square cylinder and, thus, how the heat transfer characteristics is affected by their presence.

In the literature natural convective flow about flat plate which is either vertical, horizontal or inclined, has individually received much attention because of their fundamental importance. For the present problem all these basic configurations are readily produced by the surfaces of the inner square cylinder by simply rotating the whole system about its central axis. In this case there is hydraulic and thermal interference between neighboring surfaces, of course, and it is this interference that makes the convective flow appear very interesting. In the practical view point, the present problem is also important since its result could be used to re-evaluate the performance of the conventional circular annuli in a comparative fashion.

There is much fundamental difference in the basic mechanism between the flow of natural convection and that of forced convection. In forced convection the boundary layer is produced by the solid-fluid interaction through the agency of viscosity. Its growth is suppressed by the favorable pressure gradient of the outer main stream; it is thickened and soon detached wherever the pressure gradient is adverse, since its kinetic energy is depleted rapidly by the strong viscous interaction there. On the other hand, boundary layer in the natural convection is driven by local buoyancy force distributed within the heated volume of fluid near thermal energy sources. This boundary

layer flow is likely to separate, therefore, when the component of the buoyancy force normal to the thermal surface becomes relatively large. A second important distinction between the natural and forced convection is the entrainment of ambient fluid by the boundary layer flow. In natural convection the continuity equation requires the external fluid to be entrained by the thickening thermal boundary layer. By contrast, entrainment in forced convection is, except in jet flows, observed mainly in the separated region behind bluff bodies where external fluid is introduced into the transport layer by the vortices shedded continuously or in an alternating fashion [1].

The laminar momentum convection in a viscous fluid flow about two-dimensional rectangular bodies placed in a wind tunnel has been numerically investigated by Fromm and Harlow [2]. A small numerical perturbation introduced upstream has caused asymmetric, alternate vortex shedding behind the bluff surface of the rectangular body for Reynolds number greater than 50. For a bluff body with sharp corners, as seen in the above with rectangles, separation and subsequent trailing vortices in the flow is inherent no matter how small the Reynolds number is. For the natural convective flow developed past a sharp-edged bluff body, it is not certain whether detachment of the boundary layer would occur in a considerable scale. What is known for sure at the moment is that the surface of a heated body is an energy supplier for the natural convection of the adjacent fluid medium, while the surface in a forced convection plays the role of energy dissipator through viscous friction. For the present problem, interaction among the thermally actve neighboring surfaces of the inner square cylinder and the existence of the enclosing outer circuar cylinder produce patterns of natural convection very much different from those observable in the forced convections.

To study the possible flow patterns of the boundary layers, rising plumes and recirculating vortex currents occuring in the process of natural convection heat transfer in the title enclosure, two most characteristic attitudes of symmetry are taken for consideration among the infinitely many possible angular positions of the inner square cylinder, see Fig.1.

(1) The Stand-on-Surface (SOS) Position

The line in the direction of gravity force passing through the centroid of the inner square cylinder divides the cylinder into two equal rectangles with consequential horizontal and vertical perimetric surfaces.

(2) The Stand-on-Edge (SOE) Position

The same line through the centroid divides the cylinder into two equal triangles with perimetric surfaces inclined by either 45° or-45° with respect to the direction of gravity force.

To analyze the steady Boussinesq flow for some selected Rayleigh numbers in the laminar convection regime, the aspect ratio of the cylinders was fixed and Galerkin finite element method has been used in consideration of the irregular flow domain of the present problem. Experiment has been also performed for visualization of the convection streams and for measurement of local temperatures.

2. Method of Formulation

For the given problem under consideration, no single natural coordinate system is adequate to depict the flow boundary in a simple manner. Lewis [3] has adopted Cartesian coordinates in investigation of the Navier-Stokes flow in a square cylinder driven by a

rotating concentric inner circular cylinder. Uniform meshes were preassigned on the circular boundary, which necessarily led to variable mesh system in the computational domain. It required special care not to lose accuracy due to the nonuniformity in mesh sizes. In contrast, in calculating the high Reynolds number flow past a circular cylinder Thomann and Szewzyk [4] have chosen a rectangular control volume with mixed Cartesian and cylinderical coordinate system to handle the irregular flow domain. In solving the governing equations with finite difference formulation, data transfer was made from one coordinate system to the other through matching procedures at the mesh interface with some accuracy loss. Recently, to cater for problems of arbitrary geometry in a general fashion, body-fitted coordinate system has been developed and seen spread applications [5-8]. Although mapping of physical domain of arbitrary shape onto a simple rectangular comptational domain is possible by this coordinate transformation, it requires to solve a separate set of partial differential equations of Poisson type for grid generation.

In the present study, considering the capability of handling arbitrary geometry in simple Cartesian coordinate system, the Galerkin finite element method has been selected as a tool. First we introduce nondimensional variables as follows,

$$x=x^*/R,\ y=y^*/R,\ u=\frac{u^*}{\mu/(R\rho_0)},$$
$$v=\frac{v^*}{\mu/(R\rho_0)},\ p=\frac{p^*}{\mu^2/(R^2\rho_0)}\ \text{and}$$
$$T=\frac{T^*-T_0}{T_i-T_0}.$$

The Boussinesq approximate equations expressed in dimensionless forms are

$$\frac{\partial u}{\partial x}+\frac{\partial v}{\partial y}=0 \tag{1}$$

$$u\frac{\partial u}{\partial x}+v\frac{\partial u}{\partial y}=-\frac{\partial p}{\partial x}-G_r l_x T+\left(\frac{\partial^2 u}{\partial x^2}+\frac{\partial^2 u}{\partial y^2}\right) \tag{2}$$

$$u\frac{\partial v}{\partial x}+v\frac{\partial v}{\partial y}=-\frac{\partial p}{\partial y}-G_r l_y T+\left(\frac{\partial^2 v}{\partial x^2}+\frac{\partial^2 v}{\partial y^2}\right) \tag{3}$$

$$u\frac{\partial T}{\partial x}+v\frac{\partial T}{\partial y}=\frac{1}{p_r}\left(\frac{\partial^2 T}{\partial x^2}+\frac{\partial^2 T}{\partial y^2}\right) \tag{4}$$

The fluid properties here are treated as constant and the compressibility effect is neglected everywhere except for the terms of buoyancy force. As boundary conditions, on the solid surface no-slip condition is applied and T=1 and T=0 are taken on the inner and outer cylinders, respectively. On the vertical symmetric dividing line, the conditions $u=0$, $\partial v/\partial x=0$, and $\partial T/\partial x=0$ are taken. In a finite element the unknowns are usually expressed by the approximations

$$u(x,\ y)=\sum N_j(x,y)u_j \tag{5}$$
$$v(x,\ y)=\sum N_j(x,y)v_j \tag{6}$$
$$T(x,x)=\sum N_j(x,y)T_j \tag{7}$$
$$p(x,\ y)=\sum M_j(x,y)p_j \tag{8}$$

where N and M are shape functions of quadratic and linear form, respectively. Using the Galerkin weighted residual method and Gauss-Green formula, the continuum equations can be written discretely as

$$\int_{A_e}\left[M_i\sum\frac{\partial N_k}{\partial x}u_k+M_i\sum\frac{\partial N_k}{\partial y}v_k\right]dA_e=0 \tag{9}$$

$$\int_{A_e}\Big[N_i\sum N_j u_j\sum\frac{\partial N_k}{\partial x}u_k+N_i\sum N_j v_j\sum\frac{\partial N_k}{\partial y}\cdot u_k+N_i\frac{\partial M_k}{\partial x}p_k+N_i G_r l_x\sum N_k T_k+\frac{\partial N_i}{\partial x}\sum\frac{\partial N_k}{\partial x}u_k+\frac{\partial N_i}{\partial y}\sum\frac{\partial N_k}{\partial y}u_k\Big].$$

$$dA_e=\int_{S_e}N_i\sum\frac{\partial N_k}{\partial n}u_k\,dS_e \tag{10}$$

$$\int_{A_e}\Big[N_i\Sigma N_j u_j\Sigma\frac{\partial N_k}{\partial x}v_k+N_i\Sigma N_j v_j\Sigma\frac{\partial N_k}{\partial y}\cdot v_k+N_i\frac{\partial M_k}{\partial y}p_k+N_iG_r l_y\Sigma N_k T_k+ +\frac{\partial N_i}{\partial x}\Sigma\frac{\partial N_k}{\partial x}v_k+\frac{\partial N_i}{\partial y}\Sigma\frac{\partial N_k}{\partial y}v_k\Big]\cdot dA_e=\int_{S_e}N_i\Sigma\frac{\partial N_k}{\partial n}v_k\,dS_e \quad (11)$$

$$\int_{A_e}\Big[N_i\Sigma N_j u_j\Sigma\frac{\partial N_k}{\partial x}T_k+N_i\Sigma N_j v_j\Sigma\frac{\partial N_k}{\partial y}\cdot T_k+\frac{1}{pr}\Big(\frac{\partial N_i}{\partial x}\Sigma\frac{\partial N_k}{\partial x}T_k+\frac{\partial N_i}{\partial y}\cdot\Sigma\frac{\partial N_k}{\partial y}T_k\Big)dA_e=\int_{S_e}N_i\Sigma\frac{\partial N_k}{\partial n}T_k\,dS_e \quad (12)$$

The above local element equations are now assembled to a global matrix equation of the form,

$$[C(u)+K]x=F \quad (13)$$

where C : convective matrix
K : diffusive matrix
u : velocity vector
x : vector of unknown nodal variables
F : force vector

3. Method of Solution

Among the many possible ways of solution of the above nonlinear matrix equation, following two methods are considered.

(1) Successive Substitution or Picard Iteration Method

We write Eq. (13) as

$$[C\bar{u}^{n+1}+K]\,x^{n+1}=F \quad (14)$$

Here, the vector $\bar{u}^{n+1}$ is taken as u^n, i.e. the non linear coefficient matrix is locally linearized by taking the nodal values at the previous iteration. This succssive substitution can be slightly modified by two different manipulations such

$$\bar{u}^{n+1}=\frac{1}{2}(u^n+u^{n-1}) \quad (15)$$

and

$$\bar{u}^{n+1}=\frac{1}{2}(u^n+\bar{u}^n) \quad (16)$$

as It has been found that among the above three methods the last yields the best result in stability and convergence for the natural convection in the present geometry.

(2) Newton-Raphson Method

Eq. (13) is written somewhat differently this time as

$$x^{n+1}=-J(x^n)R(x^n)+x^n \quad (17)$$

where

$$R(x)=[C(u)+K]\,x-F \quad (18)$$

$$J(x)=\partial R(x)/\partial x \quad (19)$$

The above standard form of Newton-Raphson method can be slightly modified by incorporating the earlier scheme, Eq. (16), as follows,

$$x^{n+1}=-[C(\bar{u}^{n+1})+K]\,R(x^n)+x^n \quad (20)$$

where $\bar{u}^{n+1}$ is again taken as $(u^n+\bar{u}^n)/2$. This modification has also resulted in fast convergence and manifested stability for high Rayleigh numbers.

In the above methods, one is faced to inverse the so-called global stiffness matrix which is a large, unsymmetric, sparse and, hence, poor-banded matrix. Soution algorithm for this matrix equation is usually based on bandwidth [9] or skyline storage mode [10], or more recently the frontal method [11]. The last method exhibits excellence in saving core memory and machine time for poor-banded systems of simultaneous equations, and is adopted in the present paper.

Usually, each solution was started with noflow condition in the flow domain, i.e. $u=v=0$ for $Ra<1.0\times10^5$. For higher Rayleigh numbers the results of converged solution at $Ra=1.0\times10^5$ were used as initial values. A convergence was achieved with a criterion, $||T^n-T^{n-1}||/||T^n||<\varepsilon$, where ε is a prescribed small positive value. Triangular mesh system was chosen for the present problem as shown in Fig.1. The left-hand side represents the mesh system for the SOS-Position and

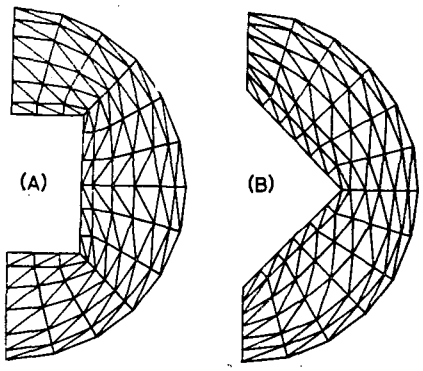

Fig. 1 Finite element mesh systems in the two symmetric convection domains: A=SOS-Position, B=SOE-Position (aspect ratio= 0.4, both).

the right hand side shows the SOE-Position. The aspect ratio, the length of a side surface of the square cylinder divided by the diameter of the circular cylinder, was fixed at 0.4 for both cases. The value of ε taken for the convergence criterion was 0.05 and in no case the iteration number exceeded eight for the Rayleigh numbers consisdered in this study.

4. Experimental Procedure

Two experimental models were constructed: one for the quantitative measurement of field temperatures, and the other mainly for flow visualization purpose. The measurement model was made of copper tubes 2-mm thick and 25-cm long. The inner square cylinder was dimensioned 4-cm in both width and depth, and the concentric outer circular cylinder of 10-cm inner diameter was shrouded with an annular cooling jacket in a similar design as in [16], where the coolant was allowed to flow helically by a long metal strip inserted in spiral form into the jacket space. The inner square cylinder was heated by a Nichrome resistance wire of 4 kΩ/m inserted inside. Fine, dried, uniformmesh metalpowder was filled around the resister wire within the square cylinder for improved uniformity of temperature in all direc tions. Regulated D.C. power supply was used to provide a constant electrical energy source. Expreiments were conducted using air kept at atmospheric pressure. Water was first used as a coolant but it was found later that air stream of room temperature was also sufficient for the various Rayleigh numbers considered in the present paper. The system normally required three to four hours before settling to a steady state. Circumferential deviation of the nondimensional temperature from the isothermality was less than 0.5% for the outer circular cylinder and 0.1% for the inner square. Maximum longitudinal deviation was registered less than 0.1%. To compare with the calculated results, temperature was measured for Rayleigh numbers higher than 5.0×10^4 in the convection space along the radial line passing through the centroid at constant azimuthal angles 0°, 45°, 90°, 135° and 180°.

The visualization model, on the other hand was made by using a plexiglass circular outer cylinder with air cooling on the surface. It allowed illumination light, which was made straight and parallel by passing through a series of lattice openings, to enter the convection space through a narrow cricumferential optical slit made on the surface of the circular cylinder. After introducing a small quantity of cooled smoke as a tracer, disturbance was rapidly transported by convection and diffusion to a quai-steady state. In this transient process toward the equilibrium, flow visualization was possible and in this respect the streamlines visualized by smoke tracer were not closed, as has been experienced also by Powe et.al. [12-13]. To avoid possible flow disturbance by the heating effect of the illumination light, visualization photgraphs were taken using

instantaneously bursting stroboscope light synchronized with the camera shutter.

5. Results and Discussion

In the present analysis, the numerical solution converged faster for the SOE-Position than the SOS and for fixed Prandtl number $Pr=0.7$ higher Rayleigh number flow was calculated for the SOE-Position. A numerical scheme generally becomes unstable, however, for Rayleigh numbers high enough, which is related with the phenomenon of laminar-to-turbulent transition. Success was made to compute the laminar convection up to $Ra=5.0\times10^5$ for the SOE-Position and up to $Ra=1.0\times10^5$ for the SOS-Position. To present the results, we define three equivalent conductivites, local, overall, and average overall as follows:

$$K_e=\frac{qLS}{k(T_i-T_0)} \tag{21}$$

$$\overline{K}_e=\frac{1}{S}\int_S K_e\ ds \tag{22}$$

$$\left(\overline{K}_e\right)_{av}=\frac{1}{2}\left[\overline{K}_e\ |\text{inner}+\overline{K}_e|\text{outer}\right] \tag{23}$$

These equivalent conductivities calculated for both inner and outer cylinders for different Rayleigh numbers are presented in Table 1. For $Ra=1.0\times10^5$, the local equivalent conductivites are graphically reproduced in Fig.2 for both SOS-and SOE-Positions. It is evident from this figure that the 90-degree sharp corners cause significant effect on the convection heat transfer. The equivalent conductivities for the outer cylinders decrease more or

Table 1 Local, mean and overall equivalent conductivities ($P_r=0.7$).

Attitude	Ra	Cylinder	Local $K_e(\phi)$							$\overline{K}_e$	$(\overline{K}_e)$av
			180°	150°	120°	90°	60°	30°	0°		
SOS	1.0×10^4	Inner	1.40	1.29	1.59	1.35	0.69	0.70	0.67	1.12	1.115
		Outer	0.62	0.67	0.61	1.29	1.66	1.37	1.53	1.11	
	5.0×10^4	Inner	2.25	2.01	2.36	2.43	1.11	0.49	0.22	1.59	1.585
		Outer	0.26	0.35	0.64	1.79	2.40	3.67	2.87	1.58	
	7.5×10^4	Inner	2.63	2.21	2.59	2.73	1.31	0.59	0.28	1.89	1.895
		Outer	0.20	0.33	0.69	1.81	2.44	3.19	4.94	1.90	
	1.0×10^5	Inner	2.83	2.38	2.75	3.00	1.50	0.63	0.33	1.99	2.000
		Outer	0.18	0.32	0.73	1.92	2.61	3.49	5.00	2.01	
SOE	1.0×10^4	Inner	1.56	1.88	1.23	1.00	1.18	0.78	0.50	1.15	1.140
		Outer	0.49	0.61	1.02	0.94	1.14	1.85	1.85	1.13	
	5.0×10^5	Inner	2.39	3.44	2.33	1.46	1.47	0.98	0.25	1.78	1.775
		Outer	0.31	0.36	0.91	1.22	2.33	3.64	3.71	1.77	
	1.0×10^5	Inner	2.71	4.22	2.95	1.84	1.67	1.16	0.27	2.13	2.140
		Outer	0.13	0.39	1.09	1.59	2.85	4.37	5.03	2.15	
	5.0×10^5	Inner	3.27	5.98	4.40	2.59	2.25	2.07	0.36	3.14	3.305
		Outer	0.18	0.44	2.05	2.55	4.11	6.00	10.1	3.47	

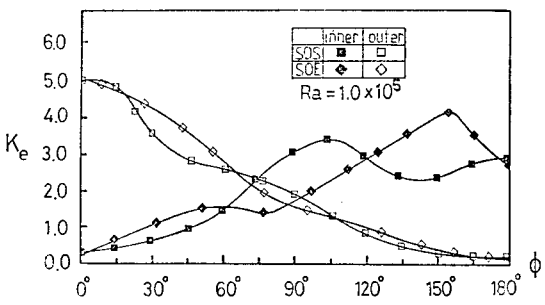

Fig. 2 Local equivalent conductivities on the cylinder surfaces, $Ra=1.0\times10^5$, $P_r=0.7$ (ϕ=azimuthal angle).

less monotonously with increasing azimuthal angle measured from the upper vertical line of symmetry, but there are slight dips in the curves at all the angles where sharp corner of the inner cylinder is located. More salient feature is manifested for the inner cylinders where large decrease in heat transfer coefficient occurs around each edged corner. It is usual that some recovery in heat transfer is followed after the depression. It is also noteworthy that the maximum heat transfer does not occur for the inner cylinders at the bottommost point, contrary to the case of circular annuli. The average overall equivalent conductivities from Table 1 can be expressed by the correlations

$$(\overline{K}_e)\,av=0.107\,\mathrm{Ra}^{0.254}\text{(SOS-Position; } 10^4\leqslant \mathrm{Ra}\leqslant 10^5) \tag{24}$$

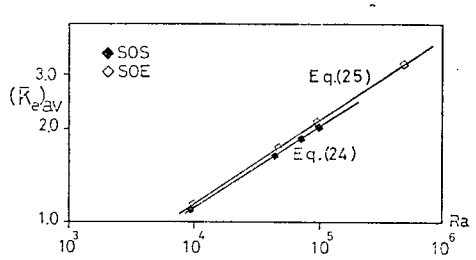

Fig. 3 Correlation curves for the overall equivalent conductivities.

$$(\overline{K}_e)\,av=0.086\,\mathrm{Ra}^{0.279}\text{(SOE-Position; } 10^4\leqslant \mathrm{Ra}\leqslant 5\times10^5) \tag{25}$$

These eqeations are plotted in logarithmic scale in Fig.3. It is clear from the above discussions and correlations that the sharp-edged corner has negative effect on the heat transfer, and the attitude of the inner square cylinder is therefore important. The SOS-Position, which has two corners in the Symmetric half of the convection space, is inferior in overall heat transfer to the SOE which has only one. For example, at $Ra=1.0\times10^5$ the inferiority is about 7%.

The overall heat transfer coefficient for low Rayleigh number flow, which is properly called pseudo-conductive by Grigull and Hauf [14], stays near that of pure conduction. In the present analysis at the lowest Rayleigh number, $Ra=1.0\times10^4$, the result could be interpreted as near pseudo-conductive since the overall equivalent conductivity is merely 1.115 for the SOS and 1.140 for the SOE. In Figs.4 and 6 for sequentially increasing Rayleigh numbers the isothermal lines are presented together with the velocity vectors shown by arrows whose maximum length is scaled to a unit. The isothermal lines at $Ra=1.0\times10^4$ are those slightly distorted from the conduction mode, although there is already a very sizable recirculating currents. These isothermal lines are more distorted from the concentric circles with increasing Rayleigh number, showing stronger influence of heated vortex. Temperature inversion occurs at this state, meaning that the fluid medium near the cooler surface is warmer than that closer to the heated surface. Now, more detailed discussions are in order about the convection patterns, differentiating the two characteristic attitudes under consideration.

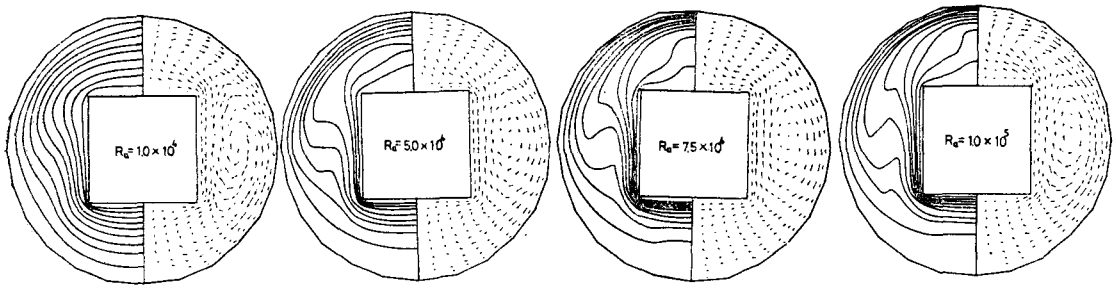

Fig. 4 Isotherms and velocity vectors at the SOS-Position.

5.1. The SOS-Position

In Fig.4, calculated results are exhibited for four different Rayleigh numbers between 1.0×10^4 and 1.0×10^5. The center of the vortex as observed by the arrows of the velocity vector is first located near central in the space between the vertical side wall of the inner square and the outer cylinder, and is raised somewhat upward with increasing Rayleigh numbers. The flow follows the contour of the sharp-edged inner heated square cylinder surprisingly well, although some small disturbances are seen locally near the sharp corners. The thermal boundary layer is well developed along most of the surfaces of the inner cylinder except on the upper horizontal wall where the temperature gradient in normal direction is very small. In this particular region the calculated result surprisingly shows no evidence of boundary layer separation at all, with no separted counter-rotating twin eddies as might be expected from the experience with forced convection. Although the flow speed is significantly retarded and the buoyancy force is directed normal to the upper surface in this region, flow separation is prevented because of the interaction with the strong thermal boundary layers from the adjacent vertical side walls. The heated boundary layers rising fast along the vertical walls entrain adjacent uflid medium in lower velocity above the upper horizontal surface, which would otherwise be stagnant or separated. Since supply of fresh fluids for entrainment cannot be continued in this region in steady state because there is no open boundary, the rising plume consequently deflects as a whole followinhg very closely the contour of the sharp-edged inner cylinder. This remarkable phenomenon produces symmetric, well-attached recirculating flows which are accelerated near the vertical side walls of the inner cylinder and retarded above the horizontal upper surface, before they stream down along the colder outer circular cylinder. Near the

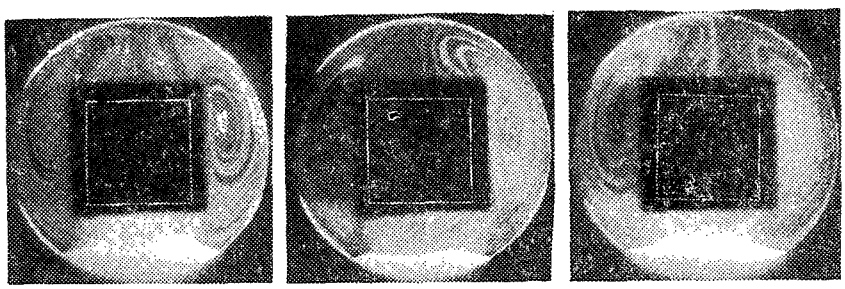

Fig. 5 Smoke streamline visualization. Rayleigh numbers: $A=7.15\times 10^4$, $B=8.06\times 10^4$, $C=1.17\times 10^5$.

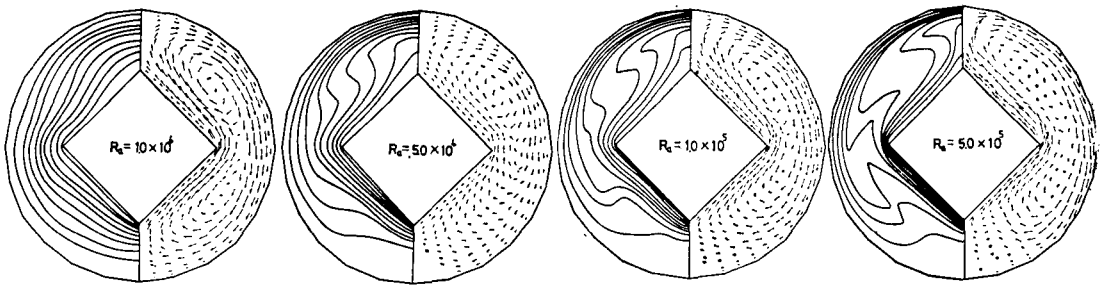

Fig. 6 Isotherms and velocity vectors at the SOE-Position.

bottom of the enclosure the fluid slows down and forms a stagnant fluid layer. The above the oretical prediction is verified by exper imental flow visualization shown in Fig.5. Smoke streamlines were photographed for three different Rayleigh numbers, 7.15×10^4, 8.06×10^4 and 1.17×10^5. The existence of symmetric recirculating flows, the dividing streamlines in the region of slowly-rising plume, and the attached flow patterns are clearly observable. The center of vortex is seen raised upward with higher Rayleigh numbers by a small distance as predicted, but the inert smoke layers in the enclosure bottom look much more distinctive than what the theoretical result tells. However, this disceepancy might be acknowledged as unavoidable because of the larger and heavier size of the smoke particles compared with the air molecules.

5. 2. The SOE-Position

The numerical simulation of the natural convection for the SOE-Position is presented in Fig. 6, where the Rayleigh number is varied from 1.0×10^4 to 5.0×10^5. For the near pseudo-conductive flow, $Ra=1.0\times10^4$, the recirculating flow in the symmetric half of the convection space has exhibited two vortex cores within one overall large rotating current. These two subvortices are circling in the same direction, and it is concluded therefore that to avoid a large shear stress between the two vortices there must be a dead flow inbetween. This dead flow occurs locally near the 90-degree edge, $\phi=90°$, making the heat transfer in this direction dominated by conduction mode, which will be quantitatively verified shortly. In contrast to the cases of the SOS-Position, for all the Rayleigth numbers considered, the thermal boundary layers are well defined everywhere along the surface of the inner cylinder including the sharp-edged corners. It is evident that this aspect contributes to the higer overall heat transfer for the

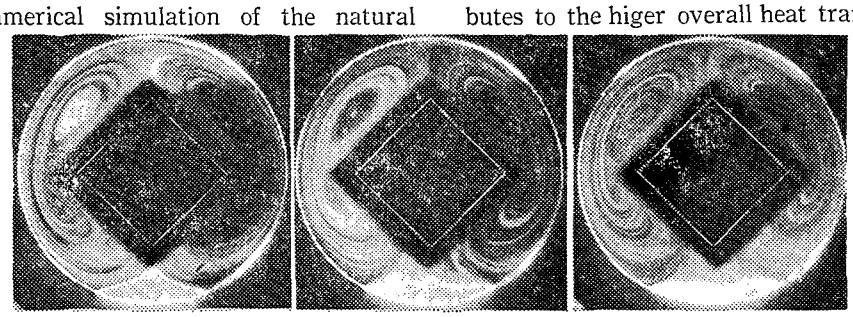

Fig. 7 Smoke streamline visualization. Rayleigh numbers: $A=3.95\times10^4$, $B=6.21\times10^4$, $C=1.05\times10^5$.

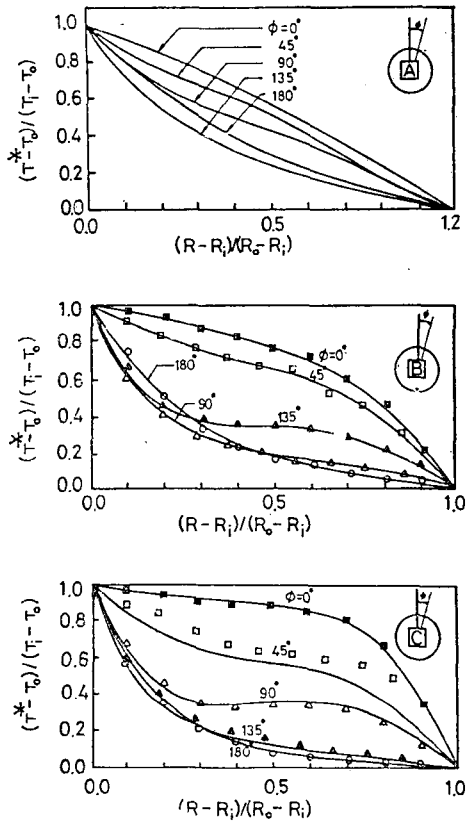

Fig. 8 Radial temperature distribution at the SOS-Position. Rayleigh numbers: $A=1.0\times10^4$ (theory), $B=5.0\times10^4$ (theory) and 5.25×10^4(exp.), $C=1.0\times10^5$(theory) and 1.10×10^5(exp.) ; —from theory and □, ■, △, ▲, ○ from measurement.

SOE-than the SOS-Position. Some slight local disturbances are seen in the velocity vectors in the flow past the sharp corner at $\phi=90°$, but again there is no evidence of separation of the boundary layer flow rising along the inclined walls of the inner cylinder. To explain the phenomenon of sharpflow-deflection without any premature separation along the heated inner cylinder, the same line of reasoning could be applied as before. Furthermore, for the present attitude of the inner cylinder the walls are inclined by either $+45°$ or $-45°$ with respect to the direciton of buoyant force, making the force component normal to the wall smaller than that of the SOS-Position. The above findings agree well qualitatively with the natural convection flow patterns obtained by the finite element method for hexagonal cylinders in Gartling [15].

The visualization photographs of tracer streamlines are shown in Fig. 7, and they verify the theoretically-predicted smaller vortices within each of the larger recirculating overall twin vortices. It is remarkable that these smaller subvortices, seen for $Ra=3.95\times10^4$ and 6.21×10^4 in the experiment and for $Ra=1.0\times10^4$ and 5.0×10^4 in the theory, emerge into a single one as the Rayleigh number is increased the lower-positioned subvortex being weakened and abosorbed by the

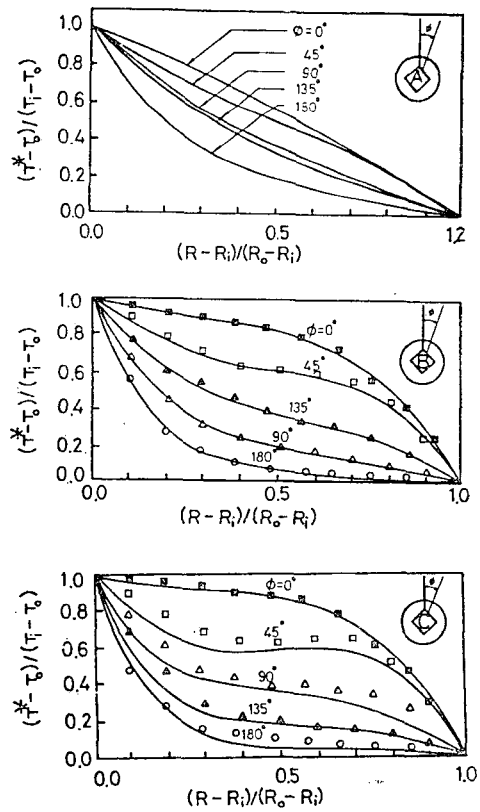

Fig. 9 Radial temperature distribution at the SOE-Position. Rayleigh numbers: $A=1.0\times10^4$ (theory), $B=5.0\times10^4$ (theory) and 6.01×10^4(exp.), $C=1.0\times10^5$(theory) and 1.15×10^5(exp.) ; —from theory and □, ■, △, ▲, ○ from measurement.

outer stronger vortex. It is found experimentally that the Rayleigh number at this critical point is approximately 6.5×10^4. For higher Rayleigh numbers, for example $Ra=5.0\times10^5$ in the theory, strong unified recirculating twin currents are formed with temperature inversion phenomenon found in almost all radial directions except near $\phi=0°$, and 180°. It is also noticed that the inert fiuid layers at the enclosure bottom have reduced size in comparson that of with the previous SOS-Position.

In Figs. 8 and 9 the radial temperature distributions calcuated and measured are presented for selected Rayleigh numbers. For $Ra=1.0\times10^4$ the computed temperature curves for both SOS-and SOE-Positions are monotonously decreasing outward and clustered around the diagonal line of negative unit slope. Especially, for the SOE-Position the temperature curve along the line $\phi=90°$ is nearly straight, revealing that the conduction effect is strongest in this direction due to the existence of the local dead flow between two subvortices, as indicated before. For high Rayleigh numbers the increased convection effect is clearly seen by the widely scattered curves with some directional indication of temperature inversion. This inversion of temperature is most distinctive along the radial line passing through the core of the large recircul ating twin vortices: for enample, in the highest Rayleigh number flows, around $\phi=90°$ for the SOS-and $\phi=45°$ for the SOE-Position. The calculated and measured temperature shows fairly good agreement for the case B's in Figs. 8 and 9 where $Ra=5.25\times10^4$ for the SOS- and $Ra=6.01\times10^4$ for the SOE-Position are taken for measurement. For the case C's, some deviation in the temperatures between the measured are seen, although the qualitative tendency is well simulated by the calculated results.

6. Concluding Remarks

In the process of achieving a settled steady-state convection heat transfer in the experiment, extraordinary care was needed for the SOS-Position to obtain streamlines of fine quality. Small disturbances of extraneous origin such as heating effect by the illumination light, small angular deviation from the exact symmetric geometrical attitude and turbulence introduced with the smoke injection, easily broke the flow symmetry and resulted in a transitional flow process with no organized characteristic convection patterns. In these cases, flows separated past sharp corners and small irregular vortices were observed above the horizontal upper surface of the inner square cylinder. This phenomenologically weak sta bility could have some connection with the earlier failure of cumputation in high Rayleigh number flow for the SOS. For carefully installed experimental systems, however, it was possible to obtain symmetric, well-attached contour-following convection currents in the laminar flow regime for the SOS-Position. For the SOE-Position, not such difficulty was faced due to stronger stability. From the discussions presented so far, following conclusions could be drawn.

(1) For the steady laminar natural convection heat transfer in the title enclosure, there is no flow separation past sharp-edged surfaces of the inner rectangular cylinder.

(2) The sharp edges play negative role in local and overall heat transfer. The SOE-Position is superior in overall heat transfer to the SOS-Position since it has only one sharp edge within a symmetric half of the convection domain compared with the two edges for the SOS.

(3) For the SOE-Position, two divided subvortices appear within each of the large overall recirculating twin currents for Rayleigh numbers roughly lower than 6.5×10^4. The subvertex in the lower position is eventually weakened and absorbed by the outer larger vortex with higher Rayleigh numbers.

Acknowledgement

The authors express their thanks to Mr. Chul H.Cho in the Department of Mechanical Engineering, KAIST, for his careful assistance with the experiment.

References

1. Gebhart, B., "Buoyancy Induced Fluid Motions Characteristic of Application in Technology-The 1978 Freeman Scholar Lecture," ASME J. of Fuids Engineering, Vol. 101, Mar. 1979, pp. 5-28.
2. Fromm, J. E., and Harlow, F. H., "Numerical Solution of the Problem of Vortex Street Development," The Physics of Fluids, Vol. 6, No, 7, July 1963, pp. 975-982.
3. Lewis, E., "Steady Flow Between a Rotating Circular Cylinder and Fixed Square Cylinder," Journal of Fluid Mechanics, Vol. 95, pt. 3, 1979, pp. 497-513.
4. Thoman, D., and Szewzyk, A. A., "Time Dependent Viscous Flow over a Circular cylinder," The physics of Fluids Supplement II, 1969, pp. 76-87.
5. Thompson, J.F, Thames, F. C., and Mastin, C.W., "Automatic Numerical Generation of Body-Fitted Curvilinear Coordinate System for Field Containing Any Number of Arbitrary Two-Dimensional Bodies," J. of Computational Physics, Vol. 15, 1974, pp. 299-319.
6. Steger, J.L., "Implicit Finite Difference Simulation of Flow About Arbitrary Two-Dimensional Geometries," AIAA J., Vol. 16, No.7, Jyly 1978, pp. 679-686.
7. Pulliam T.H., and Steger, J.L., "Implicit Finite-Difference Simulation of Three-Dimensional Compressible Flow," AIAA J., Vol.18, No.2, Feb. 1980, pp. 159-167.
8. McWhorter, J.C., III, and Sadd, M.H., "Numerical Anisotropic Heat Conduction Solutions Using Boundary-Fitted Coordinate Systems," ASME J. of Heat Transfer, Vol. 102, 1980, pp. 308-311.
9. Segelind, L.J., Applied Fnite Element Analysis, 1976, John-Wiley & Sons Inc.
10. Hasbani, Y., and Engelman, M., "Out-of-core Solution of Linear Equations with Non-symmetric Coefficient Matrix," Computers and Fluids, Vol.7, 1979 pp. 13-31.
11. Iron, B.M., "A Frontal Solution Program for Finite Element Analysis," International J. for Numerical Methods in Engineering," Vol. 2, 1970, pp. 5-32.
12. Powe, R.E., Carley, C.T., and Bishop, E.H., "Free Convective Flow Patterns in Cylindrical Annuli," ASME J. of Heat Transfer, Vol. 91, 1969, pp. 310-314.
13. Powe, R.E., Carley, C.T., and Carruth, S.L., "A Numerical Solution for Natural Convection in Cylindrical Annuli," ASME J. of Heat Transfer, Vol. 93, 1971, pp. 210-220.
14. Grigull, U., and Hauf, W., "Natural Convection in Horizontal Cylindrical Annuli," Proceedings of the Third Internaticnal Heat Transfer Conference, Paper no. 60, Vol.2, 1966, pp. 182-195.
15. Gartling, D.K., "Convective Heat Transfer Analysis by the Finite Element Method," Computer Methods in Applied Mechanics and Engineering, Vol. 12, 1977, pp. 365-382.
16. Kuehn, T.H., and Goldstein, R.J., "An Experimental Study of Natural Cenvection Heat Transfer in Concentric Horizontal Cylindrical Annuli," ASME J. of Heat Transfer, Vol. 100, 1978, pp. 635-640.